analytical chemistry

Article

pubs.acs.org/ac

Energy Charge, Redox State, and Metabolite Turnover in Single Human Hepatocytes Revealed by Capillary Microsampling Mass Spectrometry

Linwen Zhang and Akos Vertes*

Department of Chemistry, W. M. Keck Institute for Proteomics Technology and Applications, The George Washington University, Washington, District of Columbia 20052, United States

Supporting Information

ABSTRACT: Metabolic analysis of single cells to uncover cellular heterogeneity and metabolic noise is limited by the available tools. In this study, we demonstrate the utility of capillary microsampling electrospray ionization mass spectrometry with ion mobility separation for nontargeted analysis of single cells. On the basis of accurate mass measurements and collision cross-section determination, a large number of chemical species, 22 metabolites and 54 lipids, were identified. To assess the cellular response to metabolic modulators, the adenylate energy charge (AEC) levels for control and rotenone treated cells were evaluated. A significant reduction in the AEC values was observed for rotenone treated cells. For the cells under oxidative stress, the mean value for the [reduced glutathione (GSH)]/[oxidized glutathione (GSSG)] ratio was significantly decreased, whereas the distribution of the [uridine diphosphate *N*-acetylhexosamine (UDP-HexNAc)]/[uridine diphosphate hexose (UDP-hexose)] ratio exhibited dramatic tailing to higher values. Lipid turnover rates were studied by pulse-chase experiments at the single cell level.

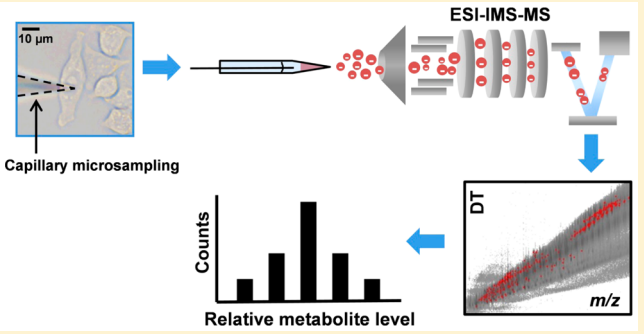

Heterogeneity of gene expression (mRNA) levels and cellular protein content is known to be common in isogenic cell populations. This variability is thought to be the result of stochastic gene expression and the low copy numbers of the corresponding chemical species in a single cell.[1,2] In turn, the cellular metabolite levels can also show large variations. Although these cell-to-cell variations are known to exist, most biochemical experiments are conducted on a large population level (millions of cells) obscuring the underlying heterogeneity and sometimes misidentifying population averages.[3,4]

Recent efforts to biochemically characterize individual cells have shown promising results in transcriptomics[5−7] and proteomics.[8−10] Beyond the general correlation between stochastic levels of mRNA and proteins, it was observed that the variability of protein levels depended on their functions.[8] For example, the proteins that respond to environmental changes exhibit larger variations than those responsible for protein synthesis. Thus, chemical analysis at a single cell level promises new insight into cellular dynamics, phenotypic variations, and the response of small cell populations to drug treatment.

The emerging field of single cell metabolomics can correlate cellular functions and physiological states.[11−14] However, identifying and quantitating a large variety of metabolites and characterizing the related metabolic noise at the single cell level is challenging due to the small sample size, fast metabolic turnover rates, dramatically wide range of concentrations, and diverse molecular structures.[13,15]

Recent reviews have thoroughly summarized the analytical advances in exploring single cell metabolomics.[16−19] Several powerful techniques, such as fluorescence microscopy[20] and stimulated Raman scattering microscopy,[21] only allow the targeted analysis of preidentified metabolites. With high sensitivity and structural elucidation capabilities, secondary ion mass spectrometry (MS) and matrix-assisted laser desorption ionization (MALDI) MS are applied for cellular and subcellular analysis of chemical species under vacuum conditions.[22,23] Heterogeneity in metabolites and energy charge of microbial cells has recently been explored by MALDI-MS.[24] Nanostructure-initiator mass spectrometry (NIMS), a matrix-free laser desorption ionization method, has also been used to analyze single cancer cells.[25,26] Currently, there is an increasing interest in combining cell micromanipulation techniques with MS for single cell analysis under ambient conditions.[27−31]

Recently, we have introduced capillary microsampling combined with electrospray ionization (ESI) and ion mobility separation (IMS) followed by MS for the metabolic analysis of single *Arabidopsis thaliana* epidermal cells with enhanced molecular coverage.[32] However, an adherent human cell often

Received: July 3, 2015
Accepted: September 23, 2015
Published: September 23, 2015

DOI: 10.1021/acs.analchem.5b02502
Anal. Chem. 2015, 87, 10397−10405

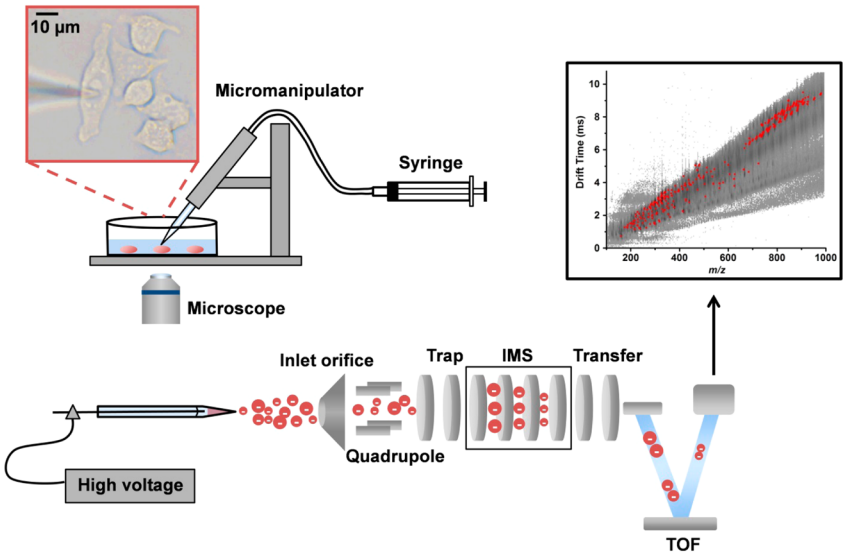

Figure 1. Schematic representation of experimental setup for single cell analysis using capillary microsampling ESI-IMS-MS. A pulled capillary held by the micromanipulator is inserted into an adherent hepatocyte (HepG2/C3A) observed through an inverted microscope. The corresponding microscope image is shown in the inset (scale bar is 10 μm). Cell content is extracted by a syringe connected to the capillary. The capillary is backfilled with electrospray solution, and the assembly is placed in front of the mass spectrometer inlet. A platinum wire is inserted into the solution, and high voltage is applied to produce an electrospray. The ions generated from the cell content are separated by the IMS system according to their DT and analyzed by the mass spectrometer. A separate DT vs m/z plot is produced for every cell.

exhibits a factor of 50−1000 lower volume than a plant cell, which makes it more challenging to obtain meaningful biological information from an individual human cell. For example, a typical human hepatocyte has a volume of <1 pL. With the help of IMS, the signal-to-noise ratio can be enhanced by elimination of phosphate buffered saline (PBS) interference and other chemical noise. Collision cross sections (CCSs), derived from IMS measurements, can provide structural information on the ions and facilitate metabolite identification with enhanced confidence.[33,34]

Stable isotope labeling, especially pulse-chase analysis, in combination with MS is often used to follow the fluxes of isotopically labeled compounds through metabolic networks within large cell populations or a multicellular organism. It helps to reconstruct incomplete metabolic networks and determine the turnover rates for specific chemical species.[35] However, in heterogeneous cell populations, the rates of metabolite and lipid turnover can vary for different subpopulations. Pulse-chase analysis at the single cell level can provide new insight into the variability of turnover rates associated with subpopulation heterogeneity.

Here, we apply capillary microsampling ESI-IMS-MS for the metabolic analysis of single human hepatocellular carcinoma cells (HepG2/C3A) and for the characterization of metabolic noise and cellular heterogeneity. Cellular physiological states, such as the energy charge and redox states, and their inherent metabolic noise levels were also characterized in cells treated by xenobiotics. Stable isotope labeling pulse-chase experiments combined with ESI-IMS-MS were performed for the analysis of lipid turnover rates in single cells.

MATERIALS AND METHODS

Chemicals. HPLC grade methanol and chloroform, dimethylsulfoxide (DMSO) (D8418, molecular biology grade, ≥99.9% purity), 98% deuterated choline chloride-(trimethyl-d_9) (492051), rotenone (45656, analytical grade), hydrogen peroxide (H_2O_2) solution (516813), adenosine triphosphate (ATP) (A2383, ≥99% purity), reduced glutathione (GSH) (G4251, premium quality, ≥98% purity), oxidized glutathione (GSSG) (G4376, premium quality, ≥98% purity), and PBS (P5368, molecular biology grade) were purchased from Sigma-Aldrich (St. Louis, MO), whereas acetic acid (≥99.0% purity) was obtained from Fluka (Seelze, Germany). Short oligomers, $3 \leq n \leq 13$, of poly-DL-alanine (P9003) from Sigma-Aldrich (St. Louis, MO), with an oligomer size distribution mainly in the $14 \leq n \leq 70$ repeat unit range, were used as calibrant in the CCS measurements. One pouch of the PBS was dissolved in 1.0 L of deionized water (18.2 MΩ·cm) to yield the 1× PBS solution used as a stock solution. Rotenone stock solution at a concentration of 1.0 mM was prepared in DMSO solvent. Choline-d_9 was dissolved in PBS solution to reach a final concentration of 10.0 mM. All chemicals were used without further purification.

Cell Culture. Human hepatocytes (HepG2/C3A) were purchased from ATCC (CRL-10741, Manassas, VA). Cells were maintained in Eagle's Minimum Essential Medium (ATCC, Manassas, VA) supplemented with 10% fetal bovine serum and 1% penicillin−streptomycin (Invitrogen, Grand Island, NY) at 37 °C and 5% CO_2 in a humidity controlled incubator (HERAcell 150i, Thermo Scientific, Waltham, MA). Viable cell numbers were determined using an automated cell counter (Countess, Invitrogen, Grand Island, NY) with trypan blue staining to reject the dead cells in the counting. Cells were seeded in 35 mm culture dishes (Corning, Tewksbury, MA) at an initial density of 2×10^5 cells/mL and raised for 12−16 h before experiments. This resulted in a cell density significantly below confluence, so individual cells could be easily identified and sampled.

To remove the medium that could cause interferences in the mass spectra, the cells were washed three times by the 0.5× PBS buffer (pH = 7.4) before single cell sampling. To study the effect of rotenone treatment, cells were exposed for 5 h to media containing 1.0 μM rotenone and compared to cells exposed only to the 0.1% DMSO vehicle as a control. For the

DOI: 10.1021/acs.analchem.5b02502
Anal. Chem. 2015, 87, 10397−10405

pulse-chase experiments, cells were cultured in a 35 mm dish with the medium containing 40 μM choline-d_9 for 36 h (pulse phase). After 36 h, the cells were washed three times by 0.5× PBS and fresh unlabeled medium was added to the dish to initiate the chase phase. Single cell analysis was performed at three time points (0, 24, and 48 h) during the chase phase.

Single Cell Sampling. Thin-wall filamented glass capillary stock (TW100F-3, World Precision Instruments, Sarasota, FL) was selected because it tends to produce larger tip openings that are suitable for mammalian cell sampling. Capillaries were pulled by a micropipette puller (P-1000, Sutter Instrument, Novato, CA) with a box filament (FB255B, Sutter Instrument, Novato, CA) using a two-step pulling program as follows. The step 1 settings were Heat = 574, Pull = 95, Velocity = 40, and Delay = 170, whereas the step 2 parameters were Heat = 564, Pull = 90, Velocity = 70, and Delay = 120 at Pressure = 500. These settings were optimized to produce capillaries with short tapering and an ∼1 μm opening. After installation of a new heating filament in the pipet puller, the parameter settings for heating, pulling, velocity, and delay time had to be reestablished for producing optimal capillaries.

Cell sampling was performed using a motorized micromanipulator (TransferMan NK2, Eppendorf, Hauppauge, NY) mounted on an inverted microscope (IX71, Olympus, Tokyo, Japan). A schematic representation of the cell sampling setup is shown in Figure 1. A capillary holder (IM-H1, Narishige, Tokyo, Japan) with the pulled capillary was mounted on the micromanipulator at 45° relative to the culture dish surface. During sampling, the capillary was carefully lowered to approach the cells of interest. As the tip was immersed into the PBS buffer, some of the solution entered into it due to capillary action. This small amount of PBS produced interfering background peaks during MS analysis. A syringe connected to the capillary holder was used to apply negative pressure to extract the cell contents into the tip. The estimated volume of the sampled cell content was ∼0.1 pL. With experience and practice, analyzing a single cell takes ∼5 min; i.e., ∼80 cells can be studied in ∼8 h. However, due to the complexity of the sampling and the limited success rate of producing a viable electrospray, a more realistic figure is ∼50 cells/day.

ESI-IMS-MS and CCS Determinations. The electrospray solution consisted of a methanol/chloroform (2:1, v/v) mixture supplemented by acetic acid to reach a final concentration of 0.1% (v/v). Analysis of large plant cells by ESI-IMS-MS has been described previously.[32] Briefly, after cell sampling, the capillary was filled from the back end with 1 μL of electrospray solution without displacing the cell sample from the front, i.e., the air had to come out through the back. Backfilling was performed by a pipet through a microloader tip (Cat. No. 930001007, Eppendorf, Hauppauge, NY), and then, the capillary was attached to an electrode holder (H-12-S, Narishige, Tokyo, Japan). A platinum wire (Alfa Aesar, Ward Hill, MA) of 100 μm in diameter and ∼5 cm in length was placed in the capillary from the back until it came in contact with the solution. The assembly was fixed at ∼5 mm away from the orifice of a quadrupole time-of-flight (TOF) mass spectrometer equipped with a traveling wave IMS system (Synapt G2-S, Waters Co., Milford, MA) (see Figure 1). A negative voltage of −2000 V was applied to the wire by a high voltage power supply (PS350, Stanford Research Systems, Inc., Sunnyvale, CA). The produced ions from cell contents were sampled by the mass spectrometer orifice and initially retained by the IMS system, where they were separated on the basis of their CCS through interactions with the drift gas. After IMS separation, the ions were further analyzed by the TOF mass spectrometer according to their mass-to-charge ratio (m/z). Nitrogen gas was supplied as the drift gas at a flow rate of 90 mL/min and a pressure of 3.25 mbar. The traveling waveform moved with a velocity of 650 m/s and had an amplitude of 40 V. The enhanced duty cycle (EDC) delay coefficient was found to be 1.41.

To distinguish and identify isobaric ions, time aligned parallel (TAP) fragmentation was performed. After the precursor ions at a particular m/z were selected by the quadrupole analyzer, they entered the IMS unit. Following separation by IMS, the isobaric ions with different drift times (DT) were fragmented by collision induced dissociation in the transfer cell. The fragmented species were resolved by the mass spectrometer according to their m/z but remained aligned with their precursor ions with respect to their DT.

Calibration of the instrument for the determination of CCS values was performed every day before the single cell experiments. For calibration, poly-DL-alanine was dissolved in 50% methanol supplemented with 0.1% acetic acid to reach a final concentration of 0.1 g/L. Singly charged poly-DL-alanine oligomers, produced by ESI, were used as the calibrant. The corresponding CCS values were found in previous publications (see Table S1).[33] Calibration curves with an $R^2 \geq 0.99$ were used for the determination of CCS values for unknown ions from single cell experiments. DriftScope 2.8 (Waters Co., Milford, MA) software was used to generate the calibration file from poly-DL-alanine data and apply automatic CCS calibration to the DT data.

Cell Lysis. To confirm the identification of chemical species and the levels of metabolite abundance ratios in single cells, metabolite and lipid extraction was performed from large cell populations following a previously published protocol.[36] Briefly, cells grown on a 60 mm dish (Corning, Tewksbury, MA) were placed in a dry ice/ethanol bath and quenched with 400 μL of methanol at −20 °C followed by 400 μL of ice cold HPLC water. The bottom of the dish was scraped by a cell scrapper to produce a cell suspension. The cells were mechanically disrupted via a syringe with a 30-gauge needle. The cell lysate was transferred into a 2 mL vial containing 400 μL of chloroform and centrifuged at 14 000g for 10 min at 4 °C (Thermo Fisher Scientific, Bremen, Germany) to produce three phases. The top phase contained the polar metabolites in the methanol solution; the bottom phase contained the nonpolar metabolites, and the lipids in the chloroform and the interphase contained the macromolecules from the cells. After transferring the top phase into another vial, the contents of both vials were dried by a vacuum concentrator (Labconco, Kansas City, MO). Before ESI-IMS-MS analysis, the polar and nonpolar cell extracts were reconstituted to 20 μL each in methanol and chloroform, respectively, and further diluted by the electrospray solution (2:1 v/v methanol/chloroform with 0.1% acetic acid).

Data Analysis. For each single cell measurement, a raw data set with ion abundances as a function of DT and m/z was collected. The DriftScope 2.8 software (Waters Co., Milford, MA) was used for visualizing the three-dimensional data sets. To reject isobaric interferences and chemical noise, different regions of the DT vs m/z plot can be selected and exported to the MassLynx 4.1 module (Waters Co., Milford, MA) for further processing of the corresponding enhanced mass spectra.

The assignments of metabolite and lipid ions from single cell analysis were based on the combination of their accurate mass

DOI: 10.1021/acs.analchem.5b02502
Anal. Chem. 2015, 87, 10397−10405

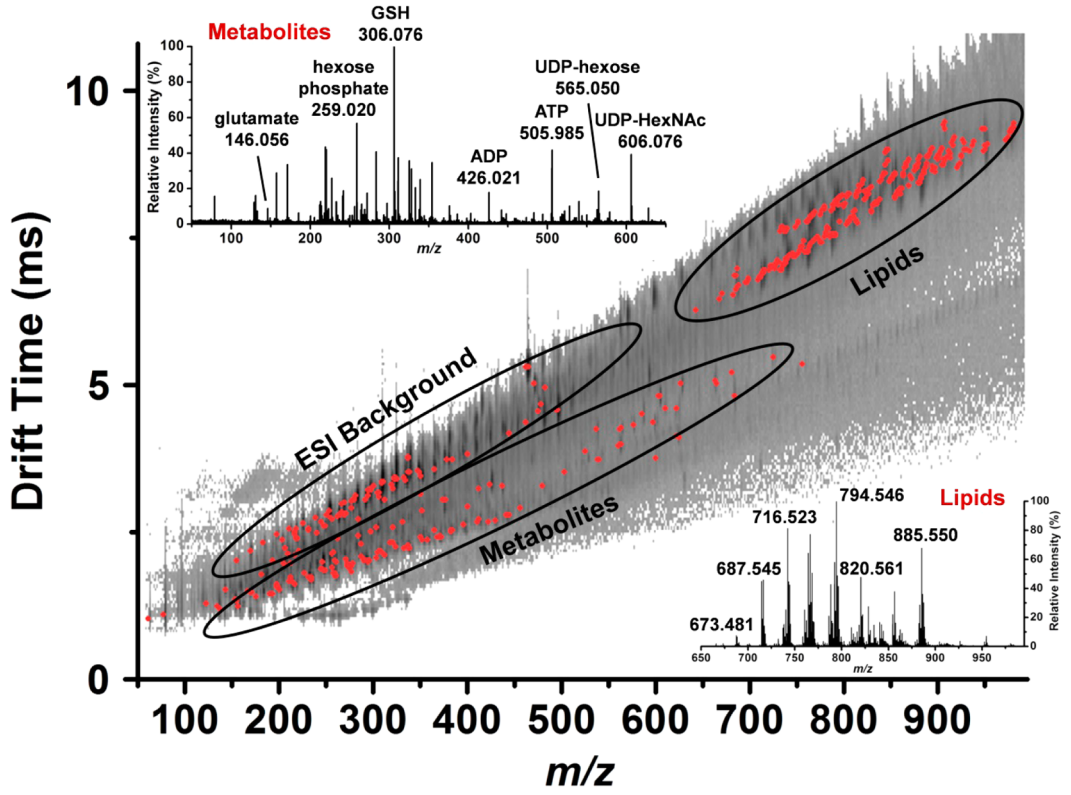

Figure 2. Identification of ion peaks (marked by red dots) are based on their m/z and CCS values (derived from their DT), and their quantitation is based on the corresponding intensities in the DT vs m/z plot. Regions highlighted by ellipses show small metabolites and lipids well separated from the ESI background ions. Corresponding mass spectra are shown in the insets with some major ion peaks labeled as follows: GSH = reduced glutathione, ADP = adenosine diphosphate, ATP = adenosine triphosphate, UDP-hexose = uridine diphosphate hexose, and UDP-HexNAc = uridine diphosphate *N*-acetylhexosamine.

values (with a mass accuracy of ±15 mDa) and the CCS measurements (with an accuracy of ±5 Å^2) (see Tables S2 and S3). To confirm the assignments, lysates of large cell populations were studied by tandem MS of the ESI generated ions through collision induced dissociation at 20−40 eV collision energies.

The NIST Isotope Calculator (ISOFORM, Version 1.02) was used to derive the calculated monoisotopic masses and visualize the isotope distribution patterns. Metabolomic and lipidomic databases, including Human Metabolome Database (http://www.hmdb.ca/), METLIN metabolite database (https://metlin.scripps.edu/), and LIPID MAPS (http://www.lipidmaps.org/), were searched to find metabolite and lipid candidates, respectively, with the mass window of 20 mDa.

RESULTS AND DISCUSSION

Metabolic Analysis of Single Human Hepatocytes by Capillary Microsampling ESI-IMS-MS. In each single cell measurement, the DT vs m/z plot was extracted for the first 3 to 5 s of the electrospray to obtain cell specific information on the metabolite and lipid ions. In Figure 2, the red dots in a representative DT vs m/z plot show the signal corresponding to ∼100 to ∼200 metabolite and lipid ions from a single cell. Due to their higher m/z and CCS characteristics, lipids are separated from metabolites in the DT vs m/z plot. Mass spectra from these two domains are shown in the insets of Figure 2. The ionic CCS values along with the accurate masses assisted in the metabolite and lipid identification. For further structural elucidation, tandem MS was performed on ions from a single cell or cell lysis samples. An example of the tandem mass spectra is shown in Figure S1. Ultimately, 22 metabolite and 54 lipid ions were identified from single cell spectra in negative ion mode (see Tables S2 and S3). The CCS measurements showed high reproducibility (relative standard deviation (RSD) < 3%) and good accuracy (ΔCCS < ±5 Å^2). The reference values for CCS were either found in the literature[33,34] or measured using chemical standards.

In Table S2, most of the assigned metabolites fall in the chemical compound classes of amino acids, e.g., glutamic acid, nucleotides, e.g., ATP, and nucleotide sugars, e.g., UDP-hexose. All the detected lipid ions in Table S3 can be assigned to the lipid classes of sphingomyelin (SM), phosphatidylcholine (PC), phosphatidic acid (PA), phosphatidylethanolamine (PE), phosphatidylserine (PS), and phosphatidylinositol (PI). To explore the structural features of the detected lipids, a plot of CCS as a function of m/z was generated on the basis of single cell data (see Figure S2). The results showed that the species with a differing number of double bonds within a lipid class were grouped together. Interestingly, the CCS values increased with the decreasing numbers of double bonds. The lipid classes in Figure S2 were partially separated and followed different trend lines. The latter could facilitate the assignment of unknown ions in complex sample analysis. For example, $[SM + Cl]^-$ and $[PC + Cl]^-$ ions showed higher CCS than other lipids with similar m/z, whereas, $[PE - H]^-$ and $[PS - H]^-$ species exhibited lower CCS values, similar to each other, over the same m/z range.

To avoid the potential bias resulting from sampling different volumes, we only characterized the ratios of ion abundances,

DOI: 10.1021/acs.analchem.5b02502
Anal. Chem. 2015, 87, 10397−10405

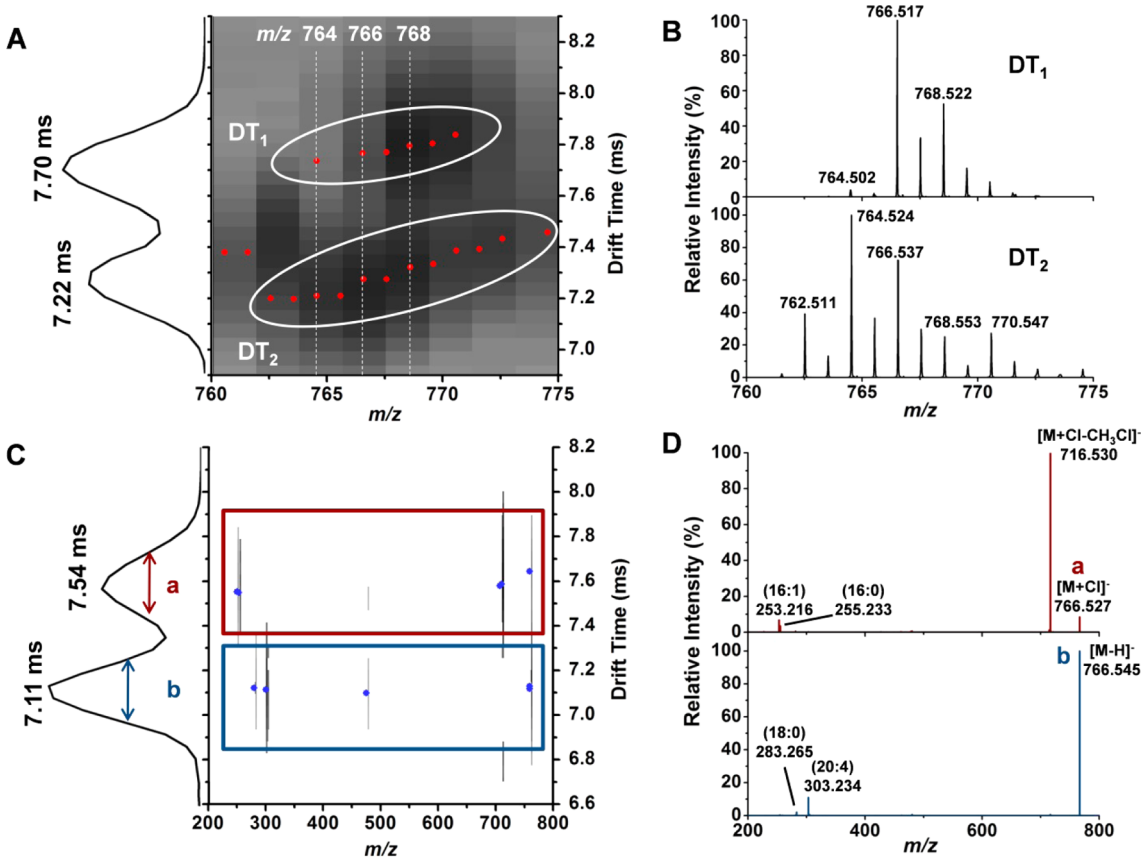

Figure 3. (A) Separating isobaric species from a single cell by IMS. The corresponding DT distributions are shown on the left, and the mass spectra extracted from the DT_1 and DT_2 regions are shown in panel (B). (C) Single cell DT vs m/z plot for the TAP fragmentation of m/z 766 isobaric species with the precursor and fragment ions marked by blue dots. The fragment peaks framed in red and blue are aligned with isobars *a* and *b* in the same DT regions, respectively. The corresponding DT distributions are represented on the left. (D) Tandem mass spectra exported from the different DT regions for isobar *a* (top) and *b* (bottom) revealed distinct fragmentation patterns consistent with $[PC(16:0/16:1) + Cl]^-$ and $[PE(18:0/20:4) - H]^-$, respectively.

which were not affected by variations in the sample volume. Intensity ratios for ions from a cell were determined for a variety of metabolites and lipids. For example, the ratio of two PC lipids, PC(16:0/18:1) (m/z 794.547, CCS = 301.1 Å^2) and PC(16:1/18:1) (m/z 792.531, CCS = 298.8 Å^2), was found to be 2.42 ± 0.63. Because of the uncertainty of the sampled volume, it is not possible to convert the ion abundances into absolute concentrations. To perform absolute quantitation would require the introduction of internal or external standards at known concentrations. In positive ion mode, a few PC lipids were detected and identified in single cells (see Table S4).

Separation and Identification of Isobaric Ions from Single Cells by Time Aligned Parallel (TAP) Fragmentation. Although the ESI signal from a cell was only available for a few seconds, efficient separation by IMS was achieved within 10 ms, enabling the differentiation of isobaric ions. For example, Figure 3A shows a zoomed DT vs m/z plot with two groups of ions separated by their DT, i.e., 7.6 ms < DT_1 < 7.9 and 7.1 ms < DT_2 < 7.5 ms. The isobaric ions indicated by the red dots at nominal m/z 764, 766, and 768 are connected by white dashed lines. The mass spectra extracted from the DT_1 and DT_2 regions showed distinct m/z values and intensity patterns (see Figure 3B). To identify the isobaric ions with nominal m/z 766, TAP fragmentation was performed after their separation by IMS. The DTs of the selected isobars and their fragments were very close to each other. The corresponding DT vs m/z plot is shown in Figure 3C with the detected isobars *a* and *b* and their fragments marked by blue dots. The dissimilar tandem mass spectra generated from the regions framed by red and blue rectangles indicate a clear distinction of the two isobars (see Figure 3D). According to the fragmentation patterns, isobar *a* was identified as $[PC(16:0/16:1) + Cl]^-$, whereas isobar *b* was assigned as $[PE(18:0/20:4) - H]^-$. Overall, with the help of TAP fragmentation, five pairs of isobaric ions were distinguished and identified from single cells.

In addition, IMS also helped to separate the PBS interference and electrospray background from the metabolite and lipid ions in single cells (see Figure S3A). Figure S3B shows that, with the help of IMS, the background noise is reduced and the signal-to-noise ratio is improved for detection of the GSSG ion with m/z 611.134. In Figure S3C, an enhanced mass spectrum for the PC lipid ions is generated by eliminating the PBS signal by IMS.

Energy Charge and Redox State Distribution Changes Due to Xenobiotics. To explore the response of the cellular energy state distribution to a metabolic modulator, the response of hepatocytes (HepG2/C3A cells) to rotenone treatment was studied using capillary microsampling ESI-IMS-MS. Rotenone, a widely used insecticide, induces cellular apoptosis by binding to complex I in the mitochondria, blocking electron transfer to ubiquinone, and eventually inhibiting the production of ATP and leading to the

DOI: 10.1021/acs.analchem.5b02502
Anal. Chem. 2015, 87, 10397−10405

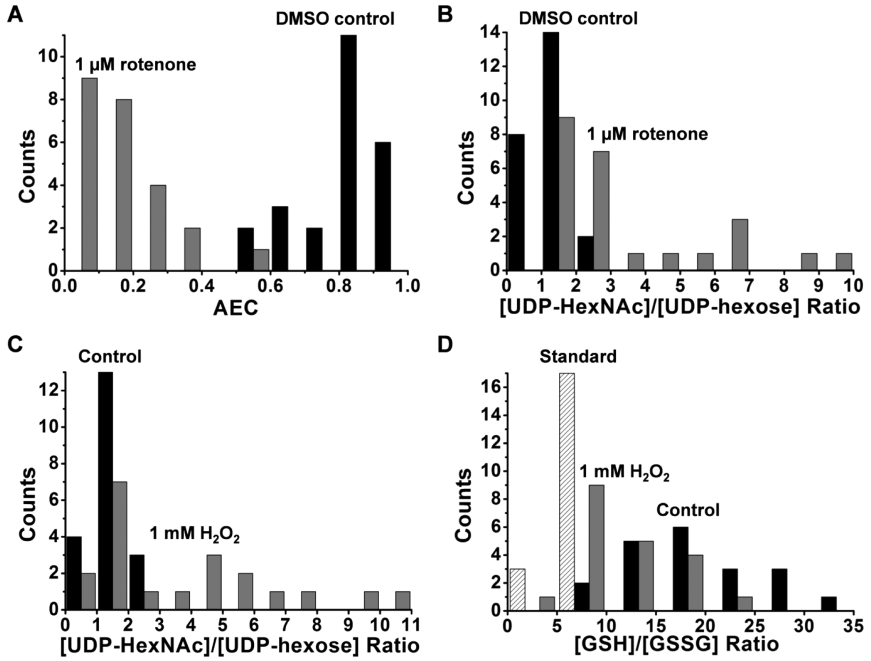

Figure 4. (A) AEC level distribution for cells in the control population containing 0.1% DMSO (black bars, t = 5 h, n = 24 cells) and cells treated by 1 μM rotenone (gray bars, t = 5 h, n = 24 cells). (B) Rotenone treatment of hepatocytes at 1 μM for t = 5 h (gray bars, n = 24 cells) results in a significant wider [UDP-HexNAc]/[UDP-hexose] distribution and a higher median value compared to the control cells (0.1% DMSO vehicle, black bars, t = 5 h, n = 24 cells). (C) Distributions of [UDP-HexNAc]/[UDP-hexose] for control cells (black bars, n = 20 cells) and cells treated by 1.0 mM H_2O_2 (gray bars, t = 1 h, n = 20 cells) indicate an upshift and significantly wider range. (D) [GSH]/[GSSG] ratio for cells from the control population (black bars) and from a sample exposed to oxidative stress caused by 1.0 mM H_2O_2 (gray bars) and similarly wide ranges were observed. Experiments on chemical standards indicated that technical variance (patterned bars) was negligible compared to cellular heterogeneity.

accumulation of mitochondrial reactive oxygen species (ROS).[37]

Adenylate energy charge (AEC), defined as ([ATP] + 0.5[ADP])/([ATP] + [ADP] + [AMP]), is an important indicator of cellular energy states. Values close to 1 indicate healthy cells, whereas low values of AEC (< ~0.5) can be indicative of cell death through an intricate interplay between apoptosis, necrosis and autophagy.[38,39] All the ion adduct forms were taken into account for calculation of the cellular AEC levels. ATP was detected in three ion adduct forms, $[M - H]^-$, $[M + Na - 2H]^-$, and $[M + K - 2H]^-$, and ADP was detected in two ion adduct forms $[M - H]^-$ and $[M + Na - 2H]^-$, whereas AMP was only detected in one ion form $[M - H]^-$. Measurements of ATP standards by ESI-IMS-MS showed that 32% of ATP decomposed to form ADP ions due to in-source fragmentation.[40] This factor was used to correct the relative abundances of ADP and ATP ions. The AEC distribution from n = 20 untreated cells shows a mean value of 0.82 ± 0.11, and the measured values exhibit a statistical range of 0.40 (see Figure S4). The mean values of AEC distributions are related to a physiological state, whereas their ranges are linked to metabolic noise.

After exposing the cells to 1.0 μM rotenone for 5 h, a significant shift in the AEC distribution was observed. Figure 4A shows that the mean value of AEC levels dramatically drops from 0.82 ± 0.12 for the cells used as control (0.1% DMSO, black bars, n = 24 cells) to 0.16 ± 0.12 for the rotenone treated population (gray bars, n = 24 cells) ($p < 6.5 \times 10^{-24}$ for the unpaired sample t test). However, the ranges of the AEC levels in the control and treated cell groups, 0.40 and 0.47, respectively, remained essentially unchanged. This means that the inherent metabolic noise of the cellular energy states is not altered by the rotenone treatment. The corresponding single cell mass spectra for untreated, control, and treated cells are shown in Figure S5A–C, respectively. Compared to the cells used as control, in the rotenone treated cells, the ATP levels were significantly reduced, GTP was not detected, and the levels of AMP and GMP were considerably elevated. This indicated that rotenone treatment induced the depletion of ATP and GTP and the accumulation of AMP and GMP.

The relative ion abundance distributions of two nucleotide sugars, UDP-hexose (m/z 565.050, CCS = 207.2 Å^2) and UDP-*N*-acetylhexosamine (UDP-HexNAc) (m/z 606.068, CCS = 222.1 Å^2), were also studied for rotenone treated and control cells. The black bars in Figure 4B show a narrow distribution for [UDP-HexNAc]/[UDP-hexose] ratios from n = 24 control cells (0.1% DMSO vehicle for 5 h) with a median value of 1.27 and a range of 2.1. Exposing the cells to 1 μM rotenone for t = 5 h (gray bars, n = 24 cells) increased the median value to 2.14 and the range to 8.1 indicating a much wider distribution. To better characterize the skewed distribution of the [UDP-HexNAc]/[UDP-hexose] ratios in rotenone treated cells, the median value was used instead of the mean. The unpaired sample t test showed significant differences between the two groups ($p < 4.7 \times 10^{-4}$).

Recent studies showed that the enzyme UDP-glucose pyrophosphorylase (UDP-Glc PPase) for the biosynthesis of UDP-Glc was inhibited by oxidative stress resulting in the reduction of UDP-Glc levels. However, the activity of UDP *N*-acetylglucosamine pyrophosphorylase (UDP-GlcNAc PPase) for UDP-GlcNAc biosynthesis was less sensitive to oxidative stress conditions.[41] Thus, the detected increased [UDP-HexNAc]/[UDP-hexose] ratios were consistent with the reduction of UDP-hexose production by the elevated ROS

DOI: 10.1021/acs.analchem.5b02502
Anal. Chem. 2015, 87, 10397−10405

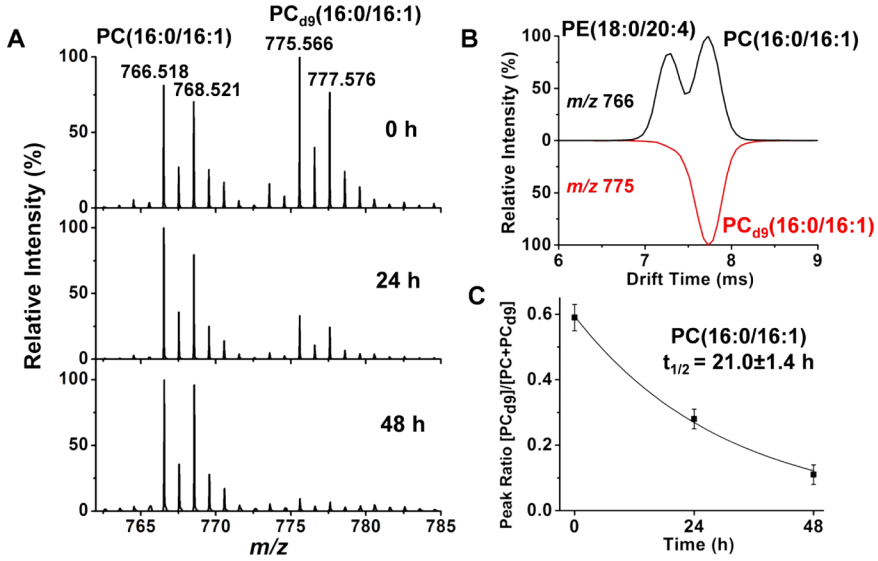

Figure 5. (A) Representative mass spectra at 0, 24, and 48 h during the chase phase indicate back conversion of the PC_{d9}(16:0/16:1) species to PC(16:0/16:1). (B) DT distributions at 0 h during the chase phase for a PC species (black trace) and the corresponding d9 labeled PC species (red trace). (C) Kinetics of the chase phase for the PC species followed exponential decay. The corresponding half-life is indicated in the figure.

levels in rotenone treated cells and with the unchanged UDP-HexNAc levels. The larger range indicated increased cellular heterogeneity in response to the oxidative stress induced by rotenone.

To confirm the role of oxidative stress in this process, [UDP-HexNAc]/[UDP-hexose] ratio distributions were studied for cells treated with 1.0 mM H_2O_2 for 1 h (see Figure 4C). Compared to cells used as control (black bars, n = 20 cells), where the median value was 1.21 with a range of 2.0, for H_2O_2 treated cells, the median value of [UDP-HexNAc]/[UDP-hexose] = 2.93 (n = 20 cells, gray bars) accompanied by a range of 10.2. The distribution in oxidative stress showed a significantly elevated median value and a dramatic increase in range ($p < 1.4 \times 10^{-3}$ for the unpaired sample t test).

To study the redox state heterogeneity in cell populations, intensity ratios of a main cellular redox buffer, [GSH]/[GSSG], were determined in individual cells. GSH was detected in $[M - H]^-$ and $[M + Na - 2H]^-$, whereas GSSG only appeared in the $[M - H]^-$ ion form. The distribution of [GSH]/[GSSG] ratios from n = 20 cells used as control is shown by black bars in Figure 4D. It exhibits a mean value of [GSH]/[GSSG] = 18.90 ± 6.68 with a range of 23.2. For the cells under oxidative stress due to 1.0 mM H_2O_2 treatment (see gray bars in Figure 4D), the mean value for the [GSH]/[GSSG] distribution was decreased to 11.42 ± 5.37 (n = 20 cells) with a range of 18.8. The statistical range remained essentially unchanged, whereas the mean values of [GSH]/[GSSG] ratios for the control group and the cells under oxidative stress were significantly different ($p < 3.9 \times 10^{-4}$ for unpaired sample t test).

To accurately assess the contributions of metabolic noise and technical variability, the latter was separately determined by measuring ion intensity ratios for a mixture of GSH and GSSG standards (bars with a pattern in Figure 4D). The ratios for the standard solutions exhibited a range of 3.0 around the mean value of [GSH]/[GSSG] = 6.2 ± 1.0 (n = 20) indicating that the variability of the single cell measurements was not altered significantly by technical factors. To confirm the relative ion abundance ratios determined in single cells, large cell population measurements were carried out on cell lysates by ESI-IMS-MS. In Table S5, a comparison of the means and medians of ion abundance ratio distributions measured from single cells with the values determined for large cell populations showed consistent results. Comparing the pairs of different ionic species in Figure 4 reveals that the [UDP-HexNAc]/[UDP-hexose] ratio distributions in rotenone treatment and under oxidative stress (Figure 4B,C, respectively) show long tails, whereas the AEC and the [GSH]/[GSSG] distributions are unskewed. Consequently, the former are best described by their medians, whereas the latter are well characterized by their mean values. Indeed, the mean of the single cell distribution and the large population value for AEC were very close to each other and they both responded with significant drops after rotenone treatment (Table S5). Likewise, the mean and the large population value for [GSH]/[GSSG] differed by only ~13%, and upon oxidative stress, they drop factors of 1.7 and 1.6, respectively. For the [UDP-HexNAc]/[UDP-hexose] ratios, the median values of single cell distributions were close to the large population results, and both showed increases in rotenone treatment and oxidative stress (see Table S5).

Lipid Turnover Rates at a Single Cell Level. To explore the heterogeneity of renewal rates for PC lipids, major components of the cell membranes, their turnover rates were studied at the single cell level. In a pulse-chase experiment, the cells were exposed to a culture medium containing 40 μM choline-d_9 for 36 h resulting in ~59% conversion of the PCs to their labeled form (pulse phase). Then, the chase phase was initiated by reversing the medium to its unlabeled form. During this phase, single cell analysis was performed in the negative ion mode at 0, 24, and 48 h time points.

Figure 5A shows the time progression of back conversion of the isotope distribution patterns from the d9 labeled form, $[PC_{d9}(16:0/16:1) + Cl]^-$, to the unlabeled form, $[PC(16:0/16:1) + Cl]^-$. To eliminate the interference from the $[PE(18:0/20:4) - H]^-$ species at nominal m/z 766 and DT = 7.22 ms, a drift time of 7.70 ms was selected in the IMS unit (see Figure 5B). This ensured that the two PC isotopolog intensities at DT = 7.70 ms were free from interference. Identification of the

DOI: 10.1021/acs.analchem.5b02502
Anal. Chem. 2015, 87, 10397−10405

isobaric ions at m/z 766 by TAP fragmentation was described above in Figure 3.

To determine the PC turnover rates, ion intensity ratios $[PC_{d9}]/[PC + PC_{d9}]$ from single cells (n = 5) were plotted as a function of time and fitted with a first-order exponential decay curve (see Figure 5C). The turnover rate and half-life of $[PC(16:0/16:1) + Cl]^-$ were found to be 0.033 ± 0.002 and 21.0 ± 1.4 h, respectively. For the saturated $[PC (16:0/16:0) + Cl]^-$ species, a turnover rate of 0.038 ± 0.003 h^{-1} and a half-life of 18.3 ± 1.4 h were obtained. The results from our single cell experiments were consistent with the half-life values of 20 to 24 h obtained for PC lipids in lysates from large cell populations.[42] The determination of molecular turnover rates in small cell groups can be used to identify and distinguish kinetically distinct subpopulations.

CONCLUSIONS

To assess the metabolic state of single human cells, we have demonstrated the analysis of a wide range of metabolite and lipid species by capillary microsampling combined with ESI-IMS-MS. Measuring multiple cells from rotenone treated and control populations, a downshift in the mean value for the AEC distributions helped to identify reduced ATP production leading to cell death through an interplay between apoptosis, necrosis and autophagy. The metabolic noise, characterized by the ranges of the AEC distributions, remained unchanged throughout this process. The [UDP-HexNAc]/[UDP-hexose] ratios showed elevated median value and broadening range due to oxidative stress, indicating increased cellular heterogeneity in response to the oxidant. Cellular response to oxidative stress in hepatocytes was followed by measuring the changes in [GSH]/[GSSG] distributions. A significant decrease of [GSH]/[GSSG] ratios was observed in the cells under oxidative stress. Results from stable isotope labeling pulse-chase experiments yielded lipid turnover rates at the single cell level.

Introducing IMS helps to increase the signal-to-noise ratio by eliminating the background ions, facilitate metabolite identification, and provide more accurate characterization of the ion abundances. As part of the general assessment of the method, we determined that ∼100 to ∼200 different ions were detected and 22 metabolites and 54 lipids were identified in a single cell. The technical and biological variability of the ion intensities were characterized by comparing cellular measurements with measurements of chemical standards under the same conditions. For example, the glutathione to oxidized glutathione ratio measured in a standard solution resulted in small variations characterized by ∼16% RSD. In contrast, the cellular measurements showed an RSD of ∼35%, indicating that the technical variance is much smaller than the biological variance.

Metabolic analysis of individual cells helps to identify the presence and gauge the degree of cellular heterogeneity. The techniques introduced in this study can reveal cellular energy and redox state distributions and their changes in response to environmental stimuli or drug treatment. Determining turnover rates for small subpopulations, selected by, e.g., flow cytometry, can highlight phenotypic differences in cell dynamics. The ability to measure metabolic noise for multiple chemical species in a cell can illuminate the role of the corresponding species in the metabolic network. Future combination of capillary microsampling with the fluorescence labeling of organelles will enable the assessment of metabolic heterogeneity on the subcellular level.

ASSOCIATED CONTENT

Supporting Information

The Supporting Information is available free of charge on the ACS Publications website at DOI: 10.1021/acs.analchem.5b02502.

Additional figures and tables (PDF)

AUTHOR INFORMATION

Corresponding Author

*E-mail: vertes@gwu.edu. Phone: +1 (202) 994-2717. Fax: +1 (202) 994-5873.

Notes

The authors declare no competing financial interest.

ACKNOWLEDGMENTS

This material is based upon work supported by the U.S. National Science Foundation under Grant No. CHE-1152302 and the George Washington University Selective Excellence Fund. The assistance of Ms. Lida Parvin with the cell cultures and Ms. Linda L. Allworth with the cell lysis experiments is greatly appreciated.

REFERENCES

(1) Elowitz, M. B.; Levine, A. J.; Siggia, E. D.; Swain, P. S. *Science* **2002**, *297*, 1183−1186.
(2) Kaern, M.; Elston, T. C.; Blake, W. J.; Collins, J. J. *Nat. Rev. Genet.* **2005**, *6*, 451−464.
(3) Altschuler, S. J.; Wu, L. F. *Cell* **2010**, *141*, 559−563.
(4) Loewer, A.; Lahav, G. *Curr. Opin. Genet. Dev.* **2011**, *21*, 753−758.
(5) Levsky, J. M.; Shenoy, S. M.; Pezo, R. C.; Singer, R. H. *Science* **2002**, *297*, 836−840.
(6) Bengtsson, M.; Stahlberg, A.; Rorsman, P.; Kubista, M. *Genome Res.* **2005**, *15*, 1388−1392.
(7) Shalek, A. K.; Satija, R.; Adiconis, X.; Gertner, R. S.; Gaublomme, J. T.; Raychowdhury, R.; Schwartz, S.; Yosef, N.; Malboeuf, C.; Lu, D. N.; Trombetta, J. J.; Gennert, D.; Gnirke, A.; Goren, A.; Hacohen, N.; Levin, J. Z.; Park, H.; Regev, A. *Nature* **2013**, *498*, 236−240.
(8) Newman, J. R. S.; Ghaemmaghami, S.; Ihmels, J.; Breslow, D. K.; Noble, M.; DeRisi, J. L.; Weissman, J. S. *Nature* **2006**, *441*, 840−846.
(9) Irish, J. M.; Kotecha, N.; Nolan, G. P. *Nat. Rev. Cancer* **2006**, *6*, 146−155.
(10) Cohen, A. A.; Geva-Zatorsky, N.; Eden, E.; Frenkel-Morgenstern, M.; Issaeva, I.; Sigal, A.; Milo, R.; Cohen-Saidon, C.; Liron, Y.; Kam, Z.; Cohen, L.; Danon, T.; Perzov, N.; Alon, U. *Science* **2008**, *322*, 1511−1516.
(11) Shrestha, B.; Vertes, A. *Anal. Chem.* **2009**, *81*, 8265−8271.
(12) Lapainis, T.; Rubakhin, S. S.; Sweedler, J. V. *Anal. Chem.* **2009**, *81*, 5858−5864.
(13) Zenobi, R. *Science* **2013**, *342*, 1243259.
(14) Nemes, P.; Rubakhin, S. S.; Aerts, J. T.; Sweedler, J. V. *Nat. Protoc.* **2013**, *8*, 783−799.
(15) Nemes, P.; Knolhoff, A. M.; Rubakhin, S. S.; Sweedler, J. V. *ACS Chem. Neurosci.* **2012**, *3*, 782−792.
(16) Amantonico, A.; Urban, P. L.; Zenobi, R. *Anal. Bioanal. Chem.* **2010**, *398*, 2493−2504.
(17) Rubakhin, S. S.; Romanova, E. V.; Nemes, P.; Sweedler, J. V. *Nat. Methods* **2011**, *8*, S20−S29.
(18) Svatos, A. *Anal. Chem.* **2011**, *83*, 5037−5044.
(19) Trouillon, R.; Passarelli, M. K.; Wang, J.; Kurczy, M. E.; Ewing, A. G. *Anal. Chem.* **2013**, *85*, 522−542.
(20) Quinn, K. P.; Sridharan, G. V.; Hayden, R. S.; Kaplan, D. L.; Lee, K.; Georgakoudi, I. *Sci. Rep.* **2013**, *3*, 3432.
(21) Freudiger, C. W.; Min, W.; Saar, B. G.; Lu, S.; Holtom, G. R.; He, C. W.; Tsai, J. C.; Kang, J. X.; Xie, X. S. *Science* **2008**, *322*, 1857−1861.

DOI: 10.1021/acs.analchem.5b02502
Anal. Chem. 2015, 87, 10397−10405

(22) Heien, M. L.; Piehowski, P. D.; Winograd, N.; Ewing, A. G. In *Mass Spectrometry Imaging: Principles and Protocols*; Rubakhin, S. S., Sweedler, J. V., Eds.; Springer: New York, 2010; Vol. *656*, pp 85−97; DOI: 10.1007/978-1-60761-746-4_4.
(23) Schober, Y.; Guenther, S.; Spengler, B.; Rompp, A. *Anal. Chem.* **2012**, *84*, 6293−6297.
(24) Ibanez, A. J.; Fagerer, S. R.; Schmidt, A. M.; Urban, P. L.; Jefimovs, K.; Geiger, P.; Dechant, R.; Heinemann, M.; Zenobi, R. *Proc. Natl. Acad. Sci. U. S. A.* **2013**, *110*, 8790−8794.
(25) Northen, T. R.; Yanes, O.; Northen, M. T.; Marrinucci, D.; Uritboonthai, W.; Apon, J.; Golledge, S. L.; Nordstrom, A.; Siuzdak, G. *Nature* **2007**, *449*, 1033−U3.
(26) O'Brien, P. J.; Lee, M.; Spilker, M. E.; Zhang, C. C.; Yan, Z.; Nichols, T. C.; Li, W.; Johnson, C. H.; Patti, G. J.; Siuzdak, G. *Cancer & metabolism* **2013**, *1*, 4.
(27) Mizuno, H.; Tsuyama, N.; Harada, T.; Masujima, T. *J. Mass Spectrom.* **2008**, *43*, 1692−1700.
(28) Fukano, Y.; Tsuyama, N.; Mizuno, H.; Date, S.; Takano, M.; Masujima, T. *Nanomedicine* **2012**, *7*, 1365−1374.
(29) Gholipour, Y.; Erra-Balsells, R.; Hiraoka, K.; Nonami, H. *Anal. Biochem.* **2013**, *433*, 70−78.
(30) Aerts, J. T.; Louis, K. R.; Crandall, S. R.; Govindaiah, G.; Cox, C. L.; Sweedler, J. V. *Anal. Chem.* **2014**, *86*, 3203−3208.
(31) Gong, X. Y.; Zhao, Y. Y.; Cai, S. Q.; Fu, S. J.; Yang, C. D.; Zhang, S. C.; Zhang, X. R. *Anal. Chem.* **2014**, *86*, 3809−3816.
(32) Zhang, L.; Foreman, D. P.; Grant, P. A.; Shrestha, B.; Moody, S. A.; Villiers, F.; Kwak, J. M.; Vertes, A. *Analyst* **2014**, *139*, 5079−5085.
(33) Paglia, G.; Williams, J. P.; Menikarachchi, L.; Thompson, J. W.; Tyldesley-Worster, R.; Halldorsson, S.; Rolfsson, O.; Moseley, A.; Grant, D.; Langridge, J.; Palsson, B. O.; Astarita, G. *Anal. Chem.* **2014**, *86*, 3985−3993.
(34) Paglia, G.; Angel, P.; Williams, J. P.; Richardson, K.; Olivos, H. J.; Thompson, J. W.; Menikarachchi, L.; Lai, S.; Walsh, C.; Moseley, A.; Plumb, R. S.; Grant, D. F.; Palsson, B. O.; Langridge, J.; Geromanos, S.; Astarita, G. *Anal. Chem.* **2015**, *87*, 1137−1144.
(35) Beisel, K. G.; Jahnke, S.; Hofmann, D.; Koppchen, S.; Schurr, U.; Matsubara, S. *Plant Physiol.* **2010**, *152*, 2188−2199.
(36) Sapcariu, S. C.; Kanashova, T.; Weindl, D.; Ghelfi, J.; Dittmar, G.; Hiller, K. *MethodsX* **2014**, *1*, 74−80.
(37) Li, N. Y.; Ragheb, K.; Lawler, G.; Sturgis, J.; Rajwa, B.; Melendez, J. A.; Robinson, J. P. *J. Biol. Chem.* **2003**, *278*, 8516−8525.
(38) Atkinson, D. E.; Walton, G. M. *J. Biol. Chem.* **1967**, *242*, 3239−3241.
(39) Atkinson, D. E. *Biochemistry* **1968**, *7*, 4030−4034.
(40) Xu, Y.; Lu, W.; Rabinowitz, J. D. *Anal. Chem.* **2015**, *87*, 2273−2281.
(41) Ebrecht, A. C.; Asencion Diez, M. D.; Piattoni, C. V.; Guerrero, S. A.; Iglesias, A. A. *Biochim. Biophys. Acta, Gen. Subj.* **2015**, *1850*, 88−96.
(42) Plageman, P. G. W. *J. Lipid Res.* **1971**, *12*, 715−724.

DOI: 10.1021/acs.analchem.5b02502
Anal. Chem. 2015, 87, 10397−10405

Supporting Information for

Energy Charge, Redox State, and Metabolite Turnover in Single Human Hepatocytes Revealed by Capillary Microsampling Mass Spectrometry

Linwen Zhang and Akos Vertes*

Department of Chemistry, W. M. Keck Institute for Proteomics Technology and Applications, The George Washington University, Washington, District of Columbia 20052, United States

*To whom correspondence should be addressed. E-mail: vertes@gwu.edu. Phone: +1 (202) 994-2717. Fax: +1 (202) 994-5873.

Supplementary Figures and Tables

Figure S1. Examples of tandem mass spectra obtained from cell lysates by ESI-IMS-MS.

Figure S2. CCS vs. *m/z* plot for lipid species from single cells.

Figure S3. A DT vs. *m/z* plot shows metabolites and lipids separated from the ESI background and the interfering ions of the PBS buffer.

Figure S4. Adenylate energy charge (AEC) distribution in untreated hepatocytes.

Figure S5. Representative mass spectra for an untreated cell, a DMSO control cell, and a rotenone treated cell.

Table S1. CCS values for singly charged protonated and deprotonated polyalanine oligomers.

Table S2. Metabolite assignments for ions from single hepatocytes in negative ion mode.

Table S3. Assignments for lipid ions measured from single hepatocytes in negative ion mode.

Table S4. Assignments for lipid ions obtained from single hepatocytes in positive ion mode.

Table S5. Metabolite abundance ratios measured in single cells and cell populations.

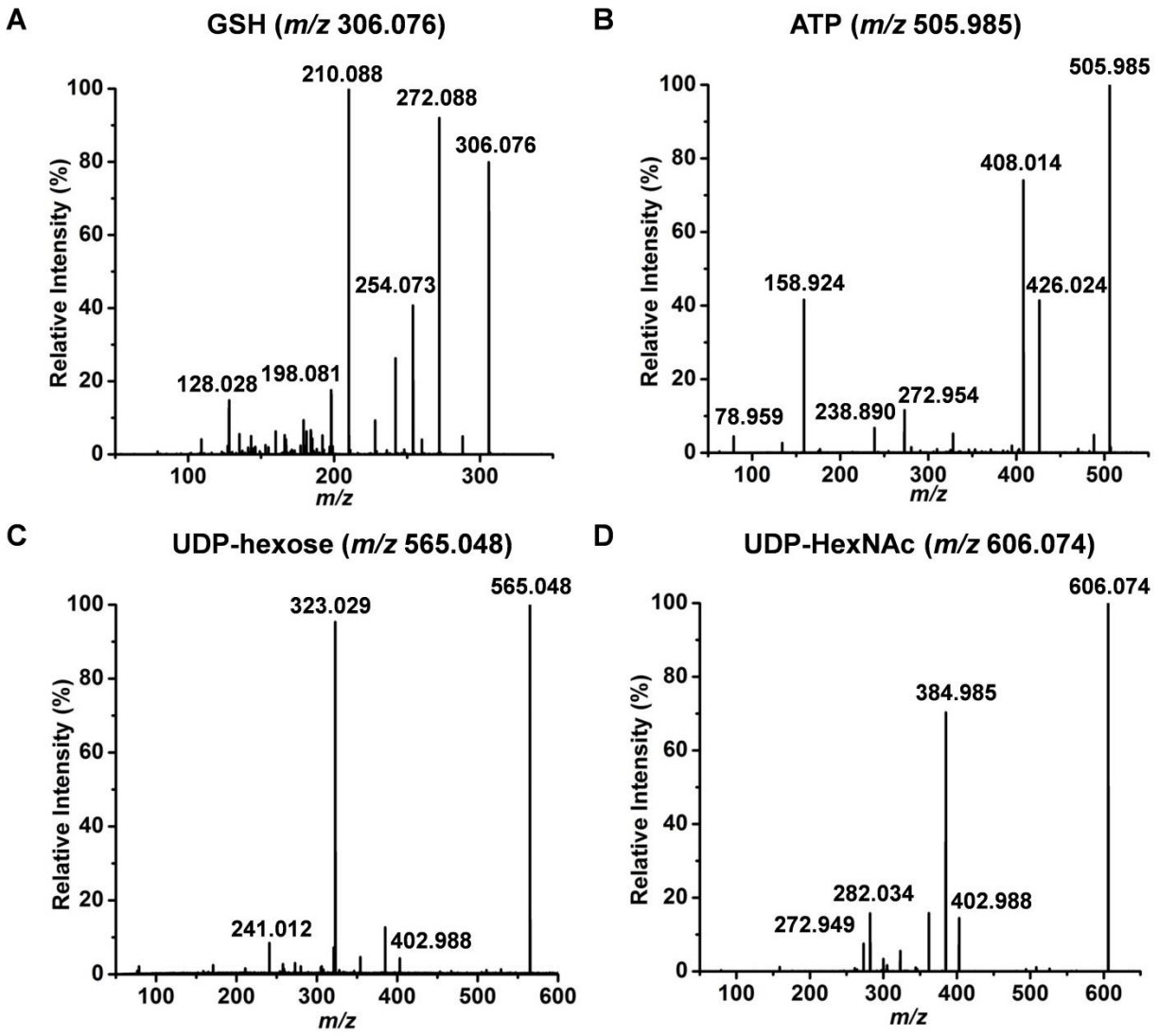

Figure S1. Tandem mass spectra for the precursor ions with (A) *m/z* 306.076, (B) *m/z* 505.985, (C) *m/z* 565.048, and (D) *m/z* 606.074 obtained from cell lysates by ESI-IMS-MS. Based on database search, such as METLIN metabolite database (https://metlin.scripps.edu/) and Human Metabolome Database (http://www.hmdb.ca/), they are identified as reduced glutathione (GSH), adenosine triphosphate (ATP), UDP-hexose, and UDP-N-acetylhexosamine (UDP-HexNAc), respectively.

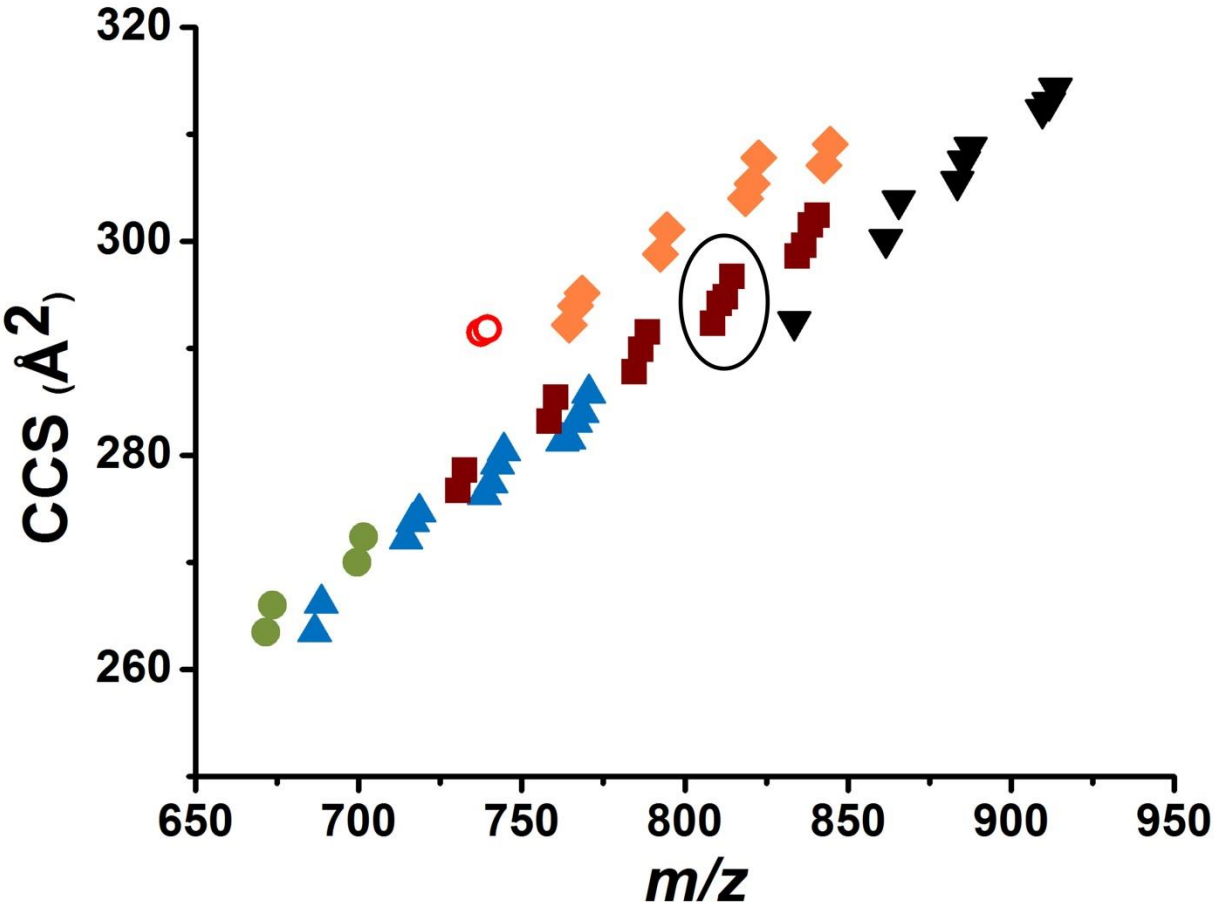

Figure S2. Partially separated lipid classes, ● [PA-H]$^-$, ▲ [PE-H]$^-$, ■ [PS-H]$^-$, ▼ [PI-H]$^-$, ◆ [PC+Cl]$^-$, and ○ [SM+Cl]$^-$, follow different trend lines in a CCS vs. *m/z* plot. Clustering within a lipid class is observed for ions with differing number of double bonds. For example, PS(18:1/20:4), PS(18:0/20:4), PS(18:0/20:3), and PS(18:1/20:1) are grouped together (see the area highlighted by an ellipse) and an increase in the number of double bonds within a group is accompanied by a reduction in the CCS. PA = phosphatidic acid, PE = phosphatidylethanolamine, PS = phosphatidylserine, PI = phosphatidylinositol, PC = phosphatidylcholine, and SM = sphingomyelin.

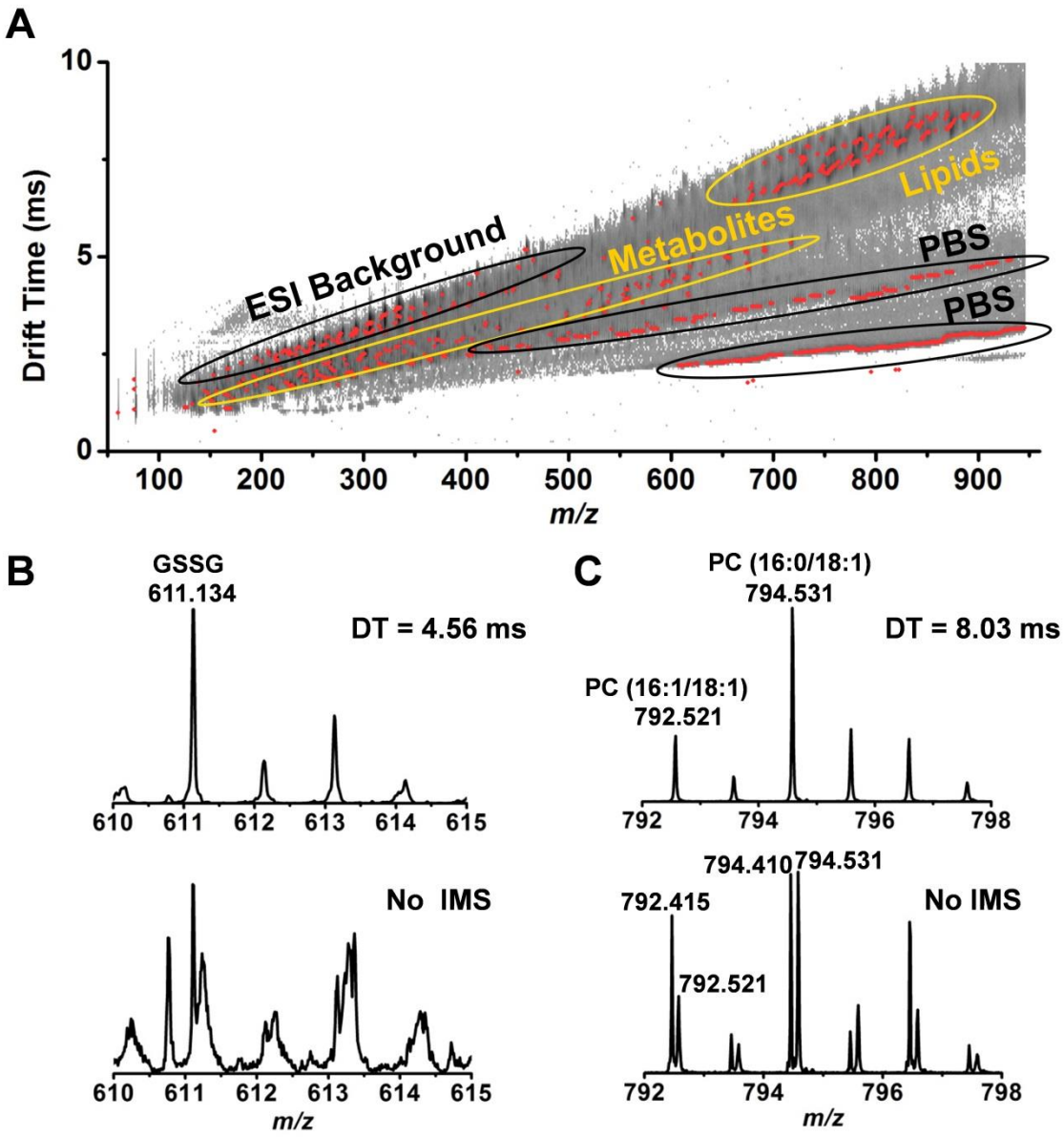

Figure S3. (A) A DT vs. *m/z* plot shows metabolite and lipid ions separated from the ESI background and the interfering ions of the PBS buffer. (B) Comparison of the mass spectra with (top panel) and without (bottom panel) IMS shows the signal-to-noise ratio is enhanced and the GSSG ion at *m/z* 611.134 is detected with IMS. (C) With the help of IMS, enhanced mass spectrum is generated for PC lipids by eliminating the interfering ions of the PBS buffer.

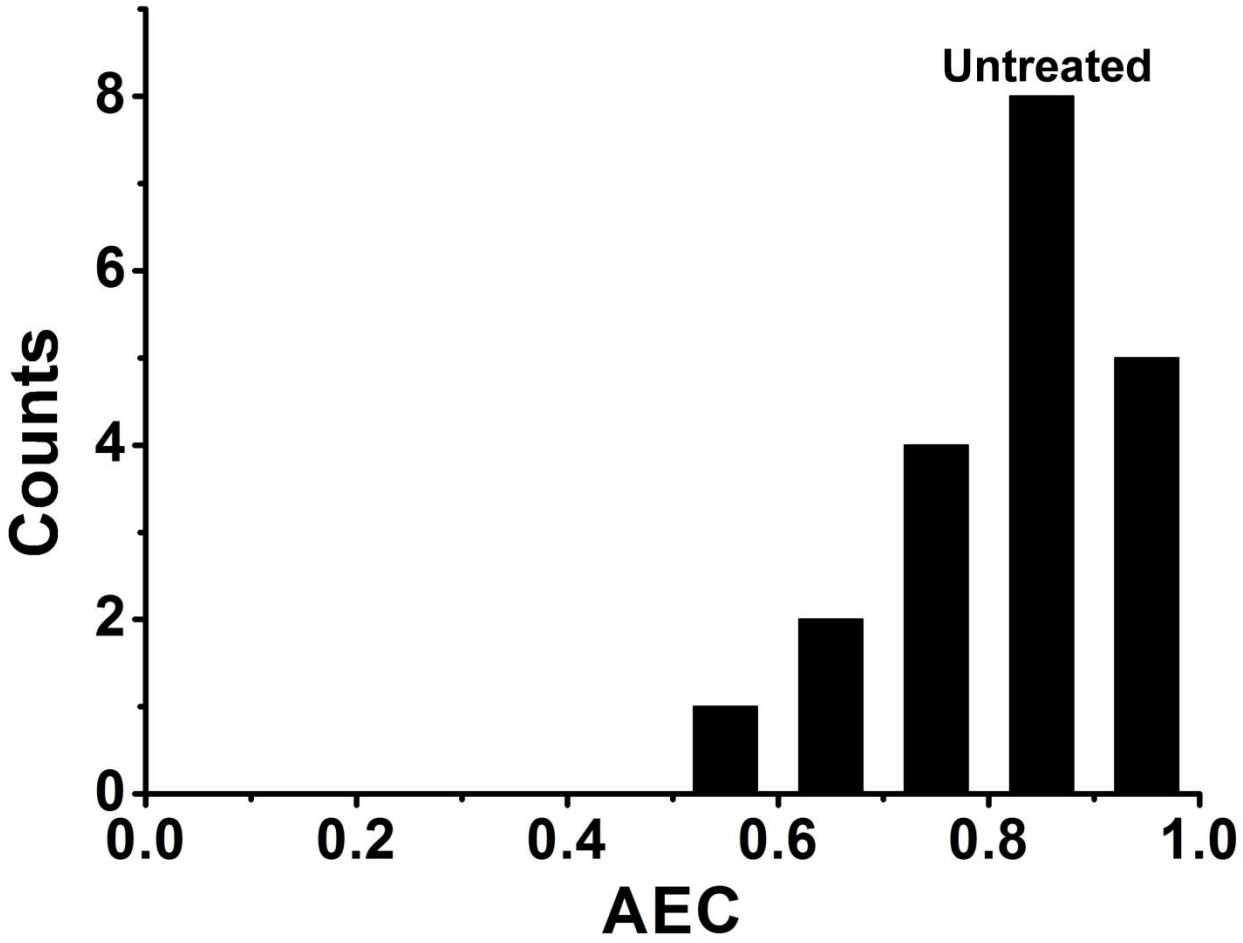

Figure S4. AEC distribution in untreated hepatocytes based on single cell measurements (n = 20) shows a mean value of 0.82±0.11 and a range of 0.40.

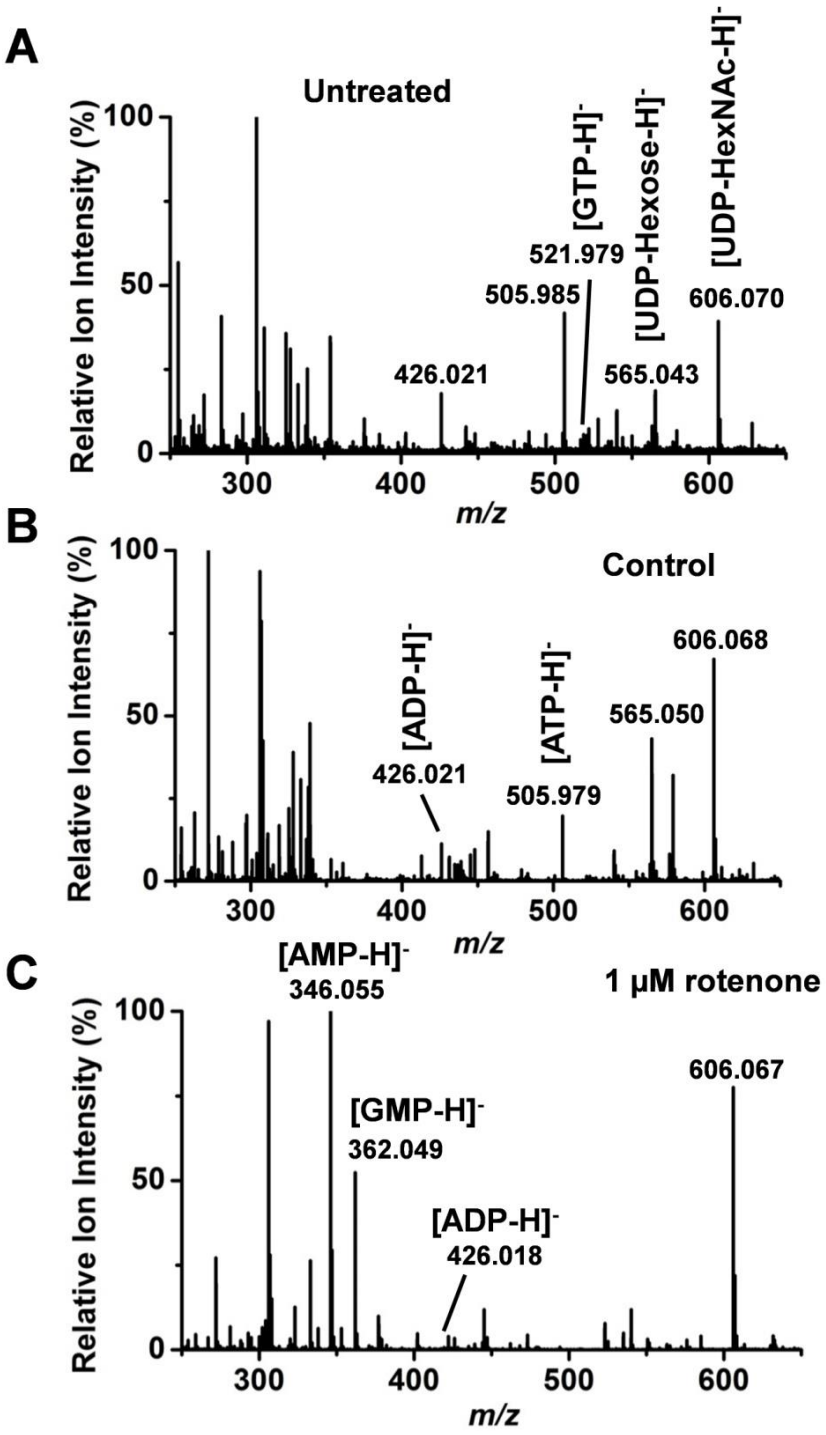

Figure S5. Representative single cell mass spectra for (A) an untreated cell, (B) a control cell in 0.1% DMSO, and (C) a rotenone treated cell.

Table S1. CCS for singly charged polyalanine oligomers with residue numbers ranging from n = 3 to n = 13 in nitrogen drift gas.[1]

n	*m/z* ($[M+H]^+$)	CCS (N_2) ($Å^2$)	*m/z* ($[M-H]^-$)	CCS (N_2) ($Å^2$)
3	232.130	151	230.114	150
4	303.167	166	301.151	165
5	374.204	181	372.188	179
6	445.241	195	443.225	195
7	516.278	211	514.262	209
8	587.315	228	585.300	223
9	658.352	243	656.337	238
10	729.390	256	727.374	253
11	800.427	271	798.411	267
12	871.464	282	869.448	279
13	942.501	294	940.485	308

Table S2. Metabolite ion assignments from single HepG2/C3A cells based on accurate mass measurements, CCS determination and tandem MS.

Name	Formula	m_{meas} (Da)	m_{calc} (Da)	Δm (mDa)	CCS_{meas} (Å^2)	CCS_{ref} (Å^2)	ΔCCS (Å^2)
adenine	$[C_5H_5N_5\text{-}H]^-$	134.041	134.047	-6	114.4	119[a]	-4.6
glutamine	$[C_5H_{10}N_2O_3\text{-}H]^-$	145.056	145.062	-6	121.4	126[a]	-4.6
glutamate	$[C_5H_9NO_4\text{-}H]^-$	146.040	146.046	-6	119.0	123[a]	-4.0
glucose/fructose phosphate	$[C_6H_{13}O_9P\text{-}H]^-$	259.020	259.022	-2	142.6	143 [a]	-0.4
reduced glutathione	$[C_{10}H_{17}N_3O_6S\text{-}H]^-$	306.076	306.076	0	158.3	159[a]	-0.7
	$[C_{10}H_{16}N_3O_6S\text{+}Na\text{-}2H]^-$	328.057	328.058	-1	159.8	160[a]	-0.2
CMP	$[C_9H_{14}N_3O_8P\text{-}H]^-$	322.042	322.045	-3	156.4	160[a]	-3.6
UMP	$[C_9H_{13}N_2O_9P\text{-}H]^-$	323.027	323.029	-2	155.6	158 [a]	-2.4
Fructose biphosphate	$[C_6H_{14}O_{12}P_2\text{-}H]^-$	338.984	338.989	-5	152.1	150[a]	2.1
AMP	$[C_{10}H_{15}N_5O_7P\text{-}H]^-$	346.053	346.056	-3	167.6	169[a]	-1.4
GMP	$[C_{10}H_{14}N_5O_8P\text{-}H]^-$	362.045	362.051	-6	163.3	165[a]	-1.7
UDP	$[C_9H_{14}N_2O_{12}P_2\text{-}H]^-$	402.994	402.995	-1	168.2	169[a]	-0.8
ADP	$[C_{10}H_{15}N_5O_{10}P_2\text{-}H]^-$	426.021	426.022	1	180.9	180[a]	0.9
	$[C_{10}H_{15}N_5O_{10}P_2\text{+}Na\text{-}2H]^-$	448.003	448.004	-1	185.0	184[b]	1.0
GDP	$[C_{10}H_{15}N_5O_{11}P_2\text{-}H]^-$	442.014	442.017	-3	176.9	178[a]	-1.1
UTP	$[C_9H_{15}N_2O_{15}P_3\text{-}H]^-$	482.953	482.961	-8	178.0		
ATP	$[C_{10}H_{16}N_5O_{13}P_3\text{-}H]^-$	505.985	505.989	-4	189.1	192[b]	-2.9
	$[C_{10}H_{16}N_5O_{13}P_3\text{+}Na\text{-}2H]^-$	527.964	527.970	-6	193.4	194[b]	-0.6
	$[C_{10}H_{16}N_5O_{13}P_3\text{+}K\text{-}2H]^-$	543.949	543.944	5	195.0	199[b]	-4.0
GTP	$[C_{10}H_{16}N_5O_{14}P_3\text{-}H]^-$	521.977	521.983	-14	191.1	190[a]	1.1
Cyclic ADP-ribose	$[C_{15}H_{21}N_5O_{13}P_2\text{-}H]^-$	540.051	540.054	-3	209.2		
UDP-hexose	$[C_{15}H_{24}N_2O_{17}P_2\text{-}H]^-$	565.050	565.048	2	207.2	204[a]	3.2
UDP glucuronic acid	$[C_{15}H_{22}N_2O_{18}P_2\text{-}H]^-$	579.019	579.027	-8	210.1		
UDP-HexNAc	$[C_{17}H_{27}N_3O_{17}P_2\text{-}H]^-$	606.068	606.074	-6	222.1		
oxidized glutathione	$[C_{20}H_{32}N_6O_{12}S_2\text{-}H]^-$	611.134	611.145	-11	219.2	218[a]	1.2
NAD	$[C_{21}H_{27}N_7O_{14}P_2\text{-}H]^-$	662.095	662.102	-7	223.0	226[a]	-3.0

[a] CCS values were obtained from the literature.[1]
[b] CCS value was obtained by measuring the corresponding chemical standard.

Table S3. Tentative assignments of lipid ions detected from single HepG2/C3A cells in negative ion mode based on accurate mass measurements, CCS determinations and tandem MS of the cell lysate. When available, the reference CCS values were obtained from a database.[2]

Lipid class	Species	Formula	m_{meas} (Da)	m_{calc} (Da)	Δm (mDa)	CCS_{meas} (Å^2)	CCS_{ref} (Å^2)	ΔCCS (Å^2)
SM	d18:1/16:0	$[C_{39}H_{79}N_2O_6P+Cl]^-$	737.535	737.537	-2	291.5		
	d18:0/16:0	$[C_{39}H_{81}N_2O_6P+Cl]^-$	739.539	739.553	-14	291.8		
PC	16:1/16:1	$[C_{40}H_{76}NO_8P+Cl]^-$	764.493	764.500	-7	292.2		
	16:0/16:1	$[C_{40}H_{78}NO_8P+Cl]^-$	766.518	766.516	2	294.0		
	16:0/16:0	$[C_{40}H_{80}NO_8P+Cl]^-$	768.521	768.531	-10	295.2		
	16:1/18:1	$[C_{42}H_{80}NO_8P+Cl]^-$	792.531	792.531	0	298.8		
	16:0/18:1	$[C_{42}H_{82}NO_8P+Cl]^-$	794.547	794.547	0	301.1		
	18:1/18:2	$[C_{44}H_{82}NO_8P+Cl]^-$	818.545	818.547	-2	304.0		
	18:1/18:1	$[C_{44}H_{84}NO_8P+Cl]^-$	820.561	820.562	-1	305.4		
	18:0/18:1	$[C_{44}H_{86}NO_8P+Cl]^-$	822.567	822.578	-11	306.8		
	18:1/20:4	$[C_{46}H_{82}NO_8P+Cl]^-$	842.547	842.547	0	307.1		
	18:1/20:3	$[C_{46}H_{84}NO_8P+Cl]^-$	844.552	844.562	-10	309.1		
PA	16:1/18:1	$[C_{37}H_{69}O_8P-H]^-$	671.467	671.466	1	263.5		
	16:0/18:1	$[C_{37}H_{71}O_8P-H]^-$	673.485	673.481	4	266.0		
	18:1/18:1	$[C_{39}H_{73}O_8P-H]^-$	699.499	699.497	2	270.0		
	18:0/18:1	$[C_{39}H_{75}O_8P-H]^-$	701.513	701.513	0	272.4		
PE	16:1/16:1	$[C_{37}H_{70}NO_8P-H]^-$	686.479	686.477	2	263.5		
	16:0/16:1	$[C_{37}H_{72}NO_8P-H]^-$	688.495	688.492	3	266.2		
	16:1/18:1	$[C_{39}H_{74}NO_8P-H]^-$	714.509	714.508	1	272.2	271	1.2
	16:0/18:1	$[C_{39}H_{76}NO_8P-H]^-$	716.524	716.524	0	273.8	272	1.8
	16:0/18:0	$[C_{39}H_{78}NO_8P-H]^-$	718.535	718.539	-4	274.7	274	0.7
	16:0/20:4	$[C_{41}H_{74}NO_8P-H]^-$	738.508	738.508	0	276.3	274	2.3
	18:1/18:2	$[C_{41}H_{76}NO_8P-H]^-$	740.523	740.524	-1	277.4	276	1.4
	18:1/18:1	$[C_{41}H_{78}NO_8P-H]^-$	742.540	742.539	1	279.2	279	0.2
	18:1/18:0	$[C_{41}H_{80}NO_8P-H]^-$	744.554	744.555	-1	280.4	281	-0.6
	16:0/22:6	$[C_{43}H_{74}NO_8P-H]^-$	762.510	762.508	2	281.3	280	1.3
	18:1/20:4	$[C_{43}H_{76}NO_8P-H]^-$	764.513	764.524	-11	281.5	283	-1.5
	18:0/20:4	$[C_{43}H_{78}NO_8P-H]^-$	766.538	766.539	-1	283.1	284	-0.9
	18:0/20:3	$[C_{43}H_{80}NO_8P-H]^-$	768.548	768.555	-7	284.0		
	18:1/20:1	$[C_{43}H_{82}NO_8P-H]^-$	770.547	770.549	-2	285.8		

PS	16:1/16:1	$[C_{38}H_{70}NO_{10}P\text{-}H]^-$	730.468	730.466	2	276.7		
	16:0/16:1	$[C_{38}H_{72}NO_{10}P\text{-}H]^-$	732.490	732.482	8	278.6		
	16:1/18:1	$[C_{40}H_{74}NO_{10}P\text{-}H]^-$	758.505	758.498	7	283.2	280	3.2
	16:1/18:0	$[C_{40}H_{76}NO_{10}P\text{-}H]^-$	760.514	760.513	1	285.4	282	3.4
	18:1/18:2	$[C_{42}H_{76}NO_{10}P\text{-}H]^-$	784.516	784.513	3	287.8	285	2.8
	18:1/18:1	$[C_{42}H_{78}NO_{10}P\text{-}H]^-$	786.528	786.529	-1	289.9	288	1.9
	18:0/18:1	$[C_{42}H_{80}NO_{10}P\text{-}H]^-$	788.536	788.545	-9	291.5	290	1.5
	18:1/20:4	$[C_{44}H_{76}NO_{10}P\text{-}H]^-$	808.514	808.513	1	292.3	290	2.3
	18:0/20:4	$[C_{44}H_{78}NO_{10}P\text{-}H]^-$	810.529	810.529	0	294.2	294	0.2
	18:0/20:3	$[C_{44}H_{80}NO_{10}P\text{-}H]^-$	812.525	812.545	-20	294.8	296	-1.2
	18:1/20:1	$[C_{44}H_{82}NO_{10}P\text{-}H]^-$	814.545	814.560	-15	296.7	298	-1.3
	18:0/22:6	$[C_{46}H_{78}NO_{10}P\text{-}H]^-$	834.529	834.529	0	298.6	300	-1.4
	18:0/22:5	$[C_{46}H_{80}NO_{10}P\text{-}H]^-$	836.533	836.545	-12	299.6	302	-2.4
	18:0/22:4	$[C_{46}H_{82}NO_{10}P\text{-}H]^-$	838.561	838.560	-1	301.5	303	-1.5
	18:1/22:2	$[C_{46}H_{84}NO_{10}P\text{-}H]^-$	840.574	840.576	-2	302.4	305	-2.6
PI	16:1/18:1	$[C_{43}H_{79}O_{13}P\text{-}H]^-$	833.517	833.519	-2	292.5	292	0.5
	18:1/18:1	$[C_{45}H_{83}O_{13}P\text{-}H]^-$	861.535	861.550	-15	300.2	300	0.2
	18:0/18:0	$[C_{45}H_{87}O_{13}P\text{-}H]^-$	865.580	865.581	-1	303.8	303	0.8
	18:1/20:4	$[C_{47}H_{81}O_{13}P\text{-}H]^-$	883.526	883.534	-8	305.6	306	-0.4
	18:0/20:4	$[C_{47}H_{83}O_{13}P\text{-}H]^-$	885.539	885.550	-11	307.5	308	-0.5
	18:0/20:3	$[C_{47}H_{85}O_{13}P\text{-}H]^-$	887.553	887.566	-13	308.8	309	-0.2
	18:1/22:5	$[C_{49}H_{83}O_{13}P\text{-}H]^-$	909.540	909.550	-10	312.3	315	-2.7
	18:1/22:4	$[C_{49}H_{85}O_{13}P\text{-}H]^-$	911.553	911.566	-13	313.0	317	-4.0
	18:1/22:3	$[C_{49}H_{87}O_{13}P\text{-}H]^-$	913.578	913.581	-3	314.3	319	-4.7

Table S4. Tentative assignments of lipid ions from single HepG2/C3A cells in positive ion mode.

Name	Formula	m_{meas} (Da)	m_{calc} (Da)	Δm (mDa)	CCS_{meas} (Å^2)
PC (16:1/16:1)	$[C_{40}H_{76}NO_8P+Na]^+$	752.518	752.520	-2	293.1
PC (16:0/16:1)	$[C_{40}H_{78}NO_8P+Na]^+$	754.536	754.536	0	296.3
PC (16:0/16:0)	$[C_{40}H_{80}NO_8P+Na]^+$	756.547	756.551	6	299.8
PC (16:1/18:1)	$[C_{42}H_{80}NO_8P+Na]^+$	780.554	780.551	3	300.1
PC (16:0/18:1)	$[C_{42}H_{82}NO_8P+Na]^+$	782.570	782.567	3	303.6
PC (18:1/18:2)	$[C_{44}H_{82}NO_8P+Na]^+$	806.573	806.567	-4	304.9
PC (18:1/18:1)	$[C_{44}H_{82}NO_8P+Na]^+$	808.588	808.583	5	308.1

Table S5. Metabolite abundance ratios measured in single cells and cell populations.

Abundance ratios	Conditions	Single Cells		Cell Population
		Mean[a]	Median[b]	
AEC	Control	0.82±0.12		0.81±0.07
	1 μM rotenone	0.16±0.12		0.22±0.03
[UDP-hexose]/[UDP-HexNAc]	Control		1.27	1.11±0.07
	1 μM rotenone		2.14	1.59±0.11
[UDP-hexose]/[UDP-HexNAc]	Control		1.21	1.15±0.05
	1 mM H_2O_2		2.93	1.44±0.02
[GSH]/[GSSG]	Control	18.90±6.68		21.35±2.51
	1 mM H_2O_2	11.42±5.37		13.44±2.13

[a] For unskewed distributions the means are more meaningful.

[b] For skewed distributions the medians are more meaningful.

REFERENCES

(1) Paglia, G.; Williams, J. P.; Menikarachchi, L.; Thompson, J. W.; Tyldesley-Worster, R.; Halldorsson, S.; Rolfsson, O.; Moseley, A.; Grant, D.; Langridge, J.; Palsson, B. O.; Astarita, G. *Anal. Chem.* **2014**, *86*, 3985-3993.
(2) Paglia, G.; Angel, P.; Williams, J. P.; Richardson, K.; Olivos, H. J.; Thompson, J. W.; Menikarachchi, L.; Lai, S.; Walsh, C.; Moseley, A.; Plumb, R. S.; Grant, D. F.; Palsson, B. O.; Langridge, J.; Geromanos, S.; Astarite, G. *Anal. Chem.* **2015**, *87*, 1137-1144.